

Provided for non-commercial research and education use.
Not for reproduction, distribution or commercial use.



This article appeared in a journal published by Elsevier. The attached copy is furnished to the author for internal non-commercial research and education use, including for instruction at the authors institution and sharing with colleagues.

Other uses, including reproduction and distribution, or selling or licensing copies, or posting to personal, institutional or third party websites are prohibited.

In most cases authors are permitted to post their version of the article (e.g. in Word or Tex form) to their personal website or institutional repository. Authors requiring further information regarding Elsevier's archiving and manuscript policies are encouraged to visit:

<http://www.elsevier.com/authorsrights>



Contents lists available at ScienceDirect

Journal of Biomechanics

journal homepage: www.elsevier.com/locate/jbiomech
www.JBiomech.com

Modeling rupture of growing aneurysms

K. Balakhovsky^a, M. Jabareen^a, K.Y. Volokh^{a,b,*}^a Faculty of Civil and Environmental Engineering, Technion – I.I.T., Israel^b Department of Structural Engineering, Ben-Gurion University of the Negev, Israel

ARTICLE INFO

Article history:

Accepted 27 November 2013

Keywords:

Aneurysms
Rupture
Modeling

ABSTRACT

Growth and rupture of aneurysms are driven by micro-structural alterations of the arterial wall yet precise mechanisms underlying the process remain to be uncovered. In the present work we examine a scenario when the aneurysm evolution is dominated by turnover of collagen fibers. In the latter case it is natural to hypothesize that rupture of individual fibers (or their bonds) causes the overall aneurysm rupture. We examine this hypothesis in computer simulations of growing aneurysms in which constitutive equations describe both collagen evolution and failure. Failure is enforced in constitutive equations by limiting strain energy that can be accumulated in a fiber. Within the proposed theoretical framework we find a range of parameters that lead to the aneurysm rupture. We conclude in a qualitative agreement with clinical observations that some aneurysms will rupture while others will not.

© 2013 Elsevier Ltd. All rights reserved.

1. Introduction

Aneurysms are abnormal dilatations of vessels in the vascular system, and they exist in two major forms: fusiform and saccular. Fusiform aneurysms are found in the human abdominal aorta. Saccular aneurysms are found in cerebral blood vessels. The Brain Aneurysm Foundation (<http://www.bafound.org/>) reports that 2 in 100 people in US have an unruptured brain aneurysm and the annual rate of rupture is about 8–10 per 100,000 people. There is a brain aneurysm rupture every 18 minutes. Ruptured brain aneurysms are fatal in about 40% of cases. Of those who survive, about 66% suffer some permanent neurological deficit. Similarly, abdominal aortic aneurysm (AAA) is found in ~2% of the elderly population, with ~150,000 new cases diagnosed each year, and the occurrence is increasing (Bengtsson et al., 1996; Ouriel et al., 1992). In many cases AAA gradually expands until rupture causing a mortality rate of 90%. The AAA rupture is considered the 13th most common cause of death in US (Patel et al., 1995).

Medical doctors consider a surgery option for enlarging AAA, for example, when its maximum diameter reaches 5.5 cm or/and expansion rate is greater than 1 cm per year. This simple geometrical criterion may possibly underestimate the risks of rupture of small aneurysms as well as overestimate the risks of rupture of large aneurysms. Biomechanical approaches to modeling aneurysm failure are desired.

Watton et al. (2004) pioneered mathematical modeling of enlarging aneurysms. They described evolution of various arterial

constituents including collagen and elastin. An interesting feature of their work is an explicit notion of the deformation corresponding to fiber recruitment. Most other fiber deformation models do not account for fiber recruitment explicitly yet introduce the phenomenon implicitly with the help of U-type (with significant stiffening) stress-strain curves. Baek et al. (2006) made another important step in modeling aneurysm growth by introducing a very convenient description of evolving strain energy density function – see formula (1) below. Building on the approaches mentioned above Kroon and Holzapfel (2007) developed aneurysm model which was attractive due to its theoretical and computational simplicity. The described works influenced further studies in mathematical modeling of aneurysm growth: Kroon and Holzapfel (2008; 2009); Chatziprodromou et al. (2007); Watton et al. (2009); Figueroa et al. (2009); Watton and Hill (2009); Schmid et al. (2010); Watton et al. (2011); and Martufi and Gasser (2012) to list a few. Though biomechanical features of intracranial and abdominal aortic aneurysms have differences (Humphrey and Taylor, 2008) the mathematical grounds of the G&R description can be common in both cases. Most mentioned theories consider turnover of collagen fibers as the main scenario of the aneurysm evolution.

Despite the success in describing growth and remodeling all mentioned theories were short of a failure description that should be a natural component of the theory. Volokh and Vorp (2008) proposed a new paradigm of Growth–Remodeling–Failure (G&R&F) by enforcing failure in a description of growth and remodeling. A failure description was enforced with the help of the *energy limiter* constant which provided a saturation value for the strain energy function (Volokh, 2011; 2013). The new constant controlled material failure and it could be interpreted as an

* Corresponding author. Tel.: +97 24 829 2426; fax: +97 24 829 5697.
E-mail address: cvolokh@technion.ac.il (K.Y. Volokh).

average energy of molecular bonds from the microstructural standpoint. It is especially noteworthy that the approach of energy limiters allowed considering *strength* independently of *stiffness*. The latter separation is critical for the aneurysm modeling where *stiffening* can be accompanied by the *loss of strength*.¹

The mentioned work by Volokh and Vorp (2008) used a purely phenomenological approach and was not guided by micro-structural considerations. Such considerations are taken into account in the present work in which we hypothesize that rupture of individual fibers (or their bonds) causes the aneurysm overall rupture. We examine this hypothesis in computer simulations of growing aneurysms in which constitutive equations describe both collagen evolution and failure. Failure is enforced in constitutive equations by limiting strain energy that can be accumulated in a fiber. Within the proposed theoretical framework we find a range of parameters that lead to aneurysm rupture. We conclude in a qualitative agreement with clinical observations that some aneurysms will rupture while others will not.

2. Methods

Most models of aneurysm growth and remodeling that appear in the works cited above, or the references therein, use fiber-based microstructural approaches. Any of these models can be enhanced with a failure description in the way it is done in the present paper. Following Humphrey and Rajagopal (2002), Baek et al. (2006), and, especially, Kroon and Holzapfel (2007) we assume that the aneurysm can be modeled as a membrane composed of collagen layers with the strain energy of the *i*th layer prescribed in the form

$$\psi_i(t) = \int_{-\infty}^t g(t, t_{dp}) \dot{m}_i(t_{dp}) f_i(t, t_{dp}) dt_{dp} \tag{1}$$

where \dot{m}_i is the rate of the collagen fiber production; f_i is the strain energy of the deposited fiber; t_{dp} is the time of the fiber deposition; and the life cycle function $g(t, t_{dp})$ is defined by the fiber life time t_{lf} with the help of the Heaviside step functions H as follows

$$g(t, t_{dp}) = H(t - t_{dp}) - H(t - t_{dp} - t_{lf}) \tag{2}$$

In order to define constitutive laws for the rate of the fiber production and the fiber energy we have, first, to define kinematics of a fiber. We assume that \mathbf{M} is a unit vector in the initial configuration at time $t = -\infty$ which defines direction of fiber deposition in the *i*th layer. Then, at time $t = t_{dp}$ a new fiber is deposited in direction

$$\mathbf{M}_{dp} = \mathbf{F}(t_{dp})\mathbf{M} \tag{3}$$

where $\mathbf{F}(t_{dp})$ is the deformation gradient mapping the initial configuration at time $t = -\infty$ to the configuration at time $t = t_{dp}$.

The deposited unit fiber $\mathbf{M}_{dp}/|\mathbf{M}_{dp}|$ is further mapped into²

$$\mathbf{m} = |\mathbf{M}_{dp}|^{-1} \mathbf{F}_{dp} \mathbf{M}_{dp} = |\mathbf{M}_{dp}|^{-1} \mathbf{F}_{dp} \mathbf{F}(t_{dp}) \mathbf{M} = |\mathbf{M}_{dp}|^{-1} \mathbf{F}(t) \mathbf{M}, \tag{4}$$

where $\mathbf{F}_{dp} = \mathbf{F}(t) \mathbf{F}^{-1}(t_{dp})$ is the deformation gradient mapping material configuration at the time of the fiber deposition $t = t_{dp}$ to the current configuration at time t .

Besides kinematics we also prescribe a specific form of the fiber strain energy function in the *i*th layer that enforces a failure description (Volokh 2011, 2013).

$$f_i(t, t_{dp}) = 0.1 \Phi_i \Gamma[0.1, 0] - \Gamma[0.1, (W_i(t, t_{dp})/\Phi_i)^{10}] \tag{5}$$

where $\Gamma[s, x] = \int_x^\infty t^{s-1} \exp(-t) dt$ is the upper incomplete gamma function; Φ_i is the energy limiter for fiber in the *i*th layer; and W_i is the strain energy of intact (without failure) fiber in the *i*th layer.

We further specify constitutive equations as follows

$$W_i(t, t_{dp}) = \mu(\lambda_{pre}^2 |\mathbf{m}|^2 - 1)^3 \tag{6}$$

$$\dot{m}_i(t_{dp}) = \beta |\mathbf{M}_{dp}|^{2\alpha} \tag{7}$$

where μ is a fiber stiffness parameter; λ_{pre} is a pre-stretch of the deposited fiber; β and α are the growth constants.

At this point the constitutive description is accomplished while a structural description is necessary. We restrict considerations by axisymmetric membranes. A

¹ Remarkably, continuum damage mechanics theories usually describe failure through decrease of stiffness while the aneurysms failure is accompanied by increase of stiffness.

² See Remark 2 below.

membrane is in equilibrium when the virtual work of internal forces, $\delta\Pi_1$, is equal to the virtual work of external forces, $\delta\Pi_2$, or

$$\delta\Pi = \delta\Pi_1 - \delta\Pi_2 = 0 \tag{8}$$

The virtual work of the internal forces can be calculated by varying the total strain energy of the membrane

$$\delta\Pi_1 = \delta \int \psi dV \tag{9}$$

where $\psi = \sum_i \psi_i$ is the strain energy density per unit reference volume V of the membrane.

The virtual work of external forces is the virtual work of pressure, p ,

$$-\delta\Pi_2 = -p \int_0^l 2\pi \mathbf{r} \mathbf{n} \cdot \delta\mathbf{x} ds = 2\pi p \int_0^l r \left(\frac{dz}{ds} \delta r - \frac{dr}{ds} \delta z \right) ds \tag{10}$$

where

$$\mathbf{n} = \begin{pmatrix} \cos \alpha \\ 0 \\ \sin \alpha \end{pmatrix} = \begin{pmatrix} -dz/ds \\ 0 \\ dr/ds \end{pmatrix}, \quad \delta\mathbf{x} = \begin{pmatrix} \delta r \\ 0 \\ \delta z \end{pmatrix} \tag{11}$$

and s is the arc length of the membrane surface – see Fig. 1.

We note that it is possible to transform integral (10) over the current configuration to the integral over a reference configuration by introducing the reference arc length, S , in a way that the current arc length is a unique function of the referential arc length: $s(S)$. After such a transformation we have

$$-\delta\Pi_2 = 2\pi p \int_0^L r(z' \delta r - r' \delta z) dS \tag{12}$$

where primes designate derivatives with respect to the referential arc length and $l = s(L)$.

Remarkably, it is possible to introduce the pressure potential explicitly (Fried, 1982)

$$-\Pi_2 = \int_0^L \gamma(r, z') dS, \quad \gamma(r, z') = p\pi r^2 z' \tag{13}$$

Indeed, varying (13) we get (12)

$$-\delta \Pi_2 = \int_0^L \left(\frac{\partial \gamma}{\partial r} \delta r - \frac{\partial^2 \gamma}{\partial S \partial z'^2} \delta z \right) dS = 2\pi p \int_0^L r(z' \delta r - r' \delta z) dS \tag{14}$$

Thus, equilibrium is provided by the stationary state of the total potential

$$\Pi = \Pi_1 - \Pi_2 = \int \psi dV + p\pi \int_0^L r^2 z' dS \tag{15}$$

This problem is conservative!

In the case of a membrane comprising n thin layers we can further simplify (15) as follows:

$$\Pi = \pi \int_0^L \left(2R \sum_{i=1}^n h_i \psi_i + p r^2 z' \right) dS \tag{16}$$

where R is the referential or initial radial coordinate; h_i and ψ_i are the thickness and the strain energy of the *i*th layer accordingly.

We can specify equations written above by describing deformation in principal stretches

$$\mathbf{F} = \lambda_1 \boldsymbol{\tau} \otimes \boldsymbol{\tau}_0 + \lambda_2 \boldsymbol{\omega} \otimes \boldsymbol{\omega}_0 + \lambda_3 \mathbf{n} \otimes \mathbf{n}_0 \tag{17}$$

where

$$\lambda_1 = s' = \sqrt{r'^2 + z'^2}, \quad \lambda_2 = \frac{2\pi r}{2\pi R} = \frac{r}{R}, \quad \lambda_3 = \frac{1}{\lambda_1 \lambda_2} \tag{18}$$

$$\boldsymbol{\tau} = \begin{pmatrix} \sin \alpha \\ 0 \\ -\cos \alpha \end{pmatrix} = \begin{pmatrix} dr/ds \\ 0 \\ dz/ds \end{pmatrix},$$

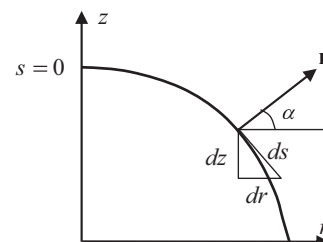


Fig. 1. Membrane of revolution.

$$\boldsymbol{\omega} = \mathbf{n} \times \boldsymbol{\tau} = \begin{pmatrix} 0 \\ 1 \\ 0 \end{pmatrix}, \quad \mathbf{n} = \begin{pmatrix} \cos \alpha \\ 0 \\ \sin \alpha \end{pmatrix} = \begin{pmatrix} -dz/ds \\ 0 \\ dr/ds \end{pmatrix} \quad (19)$$

$$\boldsymbol{\tau}_0 = \begin{pmatrix} \sin \alpha_0 \\ 0 \\ -\cos \alpha_0 \end{pmatrix} = \begin{pmatrix} dR/dS \\ 0 \\ dZ/dS \end{pmatrix},$$

$$\boldsymbol{\omega}_0 = \mathbf{n}_0 \times \boldsymbol{\tau}_0 = \begin{pmatrix} 0 \\ 1 \\ 0 \end{pmatrix}, \quad \mathbf{n}_0 = \begin{pmatrix} \cos \alpha_0 \\ 0 \\ \sin \alpha_0 \end{pmatrix} = \begin{pmatrix} -dZ/dS \\ 0 \\ dR/dS \end{pmatrix} \quad (20)$$

Eqs. (17)–(20) use current quantities $r, z, s, \alpha, \boldsymbol{\tau}, \boldsymbol{\omega}, \mathbf{n}$ and their referential counterparts $R, Z, S, \alpha_0, \boldsymbol{\tau}_0, \boldsymbol{\omega}_0, \mathbf{n}_0$ accordingly.

Besides, we define the referential fiber direction by using fiber angle ϕ_i of the i th layer

$$\mathbf{M} = \cos \phi_i \boldsymbol{\tau}_0 + \sin \phi_i \boldsymbol{\omega}_0 \quad (21)$$

Based on (17) and (21) we find

$$|\mathbf{M}_{dp}|^2 = \lambda_1^2(t_{dp}) \cos^2 \phi_i + \lambda_2^2(t_{dp}) \sin^2 \phi_i \quad (22)$$

$$|\mathbf{m}|^2 = \frac{\lambda_1^2(t) \cos^2 \phi_i + \lambda_2^2(t) \sin^2 \phi_i}{\lambda_1^2(t_{dp}) \cos^2 \phi_i + \lambda_2^2(t_{dp}) \sin^2 \phi_i} \quad (23)$$

Substituting (22),(23) in (6),(7) we have finally constitutive laws in terms of principal stretches

$$W_i(t, t_{dp}) = \mu \left(\lambda_{pre}^2 \frac{\lambda_1^2(t) \cos^2 \phi_i + \lambda_2^2(t) \sin^2 \phi_i}{\lambda_1^2(t_{dp}) \cos^2 \phi_i + \lambda_2^2(t_{dp}) \sin^2 \phi_i} - 1 \right)^3 \quad (24)$$

$$\dot{m}_i(t_{dp}) = \beta (\lambda_1^2(t_{dp}) \cos^2 \phi_i + \lambda_2^2(t_{dp}) \sin^2 \phi_i)^\alpha \quad (25)$$

Spatial-temporal discretization is discussed in Appendix A.

We consider two geometries for two sorts of aneurysm.

The first is a circular membrane (fixed at the edge) which mimics saccular intracranial aneurysm. The membrane has radius $R_0 = 2.5$ mm and thickness $T = 30$ μ m. It inflates under pressure gradually increasing up to $P = 7$ KPa and evolves in accordance with the constitutive law. Other parameters are $\lambda_{pre} = 1.02$, $t = 200t_{lf}$, $\mu = 2 \times 10^7$ Pa, $\alpha = 2$ and $\beta t_{lf} = 0.486$. We assume 4 layers of fibers of uniform thickness $T_i = T/4$. The fibers are oriented in directions $\phi_1 = 0$, $\phi_2 = \pi/4$, $\phi_3 = \pi/2$ and $\phi_4 = 3\pi/4$ in the reference configuration. In choosing the values of parameters we followed Kroon and Holzapfel (2007) who discussed the choice in detail and we will not duplicate the discussion here.

The second geometry is a cylinder. The cylindrical axisymmetric membrane mimics fusiform aneurysm. It has radius $R_0 = 10$ mm, height $H = 25$ mm and thickness $T = 1.0$ mm. Pressure used for this model is $P = 16$ KPa. We slightly changed the values of parameters to better fit abdominal aortic aneurysms. Other material parameters are the same as for the circular membrane.

In the absence of precise experimental data and in view of its natural scattering parametric studies are needed and they are presented in the next section.

Remark 1. Aneurysms start enlarging with degradation of elastin so it is not unreasonable to assume that collagen dominates aneurysm growth from the start. Probably, some transition period exists at the beginning of aneurysm growth when elastin degrades while its presence is still significant. Unluckily, aneurysms are identified when they are already developed so it is difficult to assess the transition stage experimentally.

Remark 2. We introduced the energy limiter in the constitutive theory proposed by Kroon and Holzapfel (2007) who championed simplicity. However, we deviated from their formulation in Eq. (4), which would originally read $\mathbf{m} = \mathbf{F}_{dp} \mathbf{M}$ according to Kroon and Holzapfel (2007, Eq. (2)). We modified the original formulation because \mathbf{F}_{dp} and \mathbf{M} belong to different configurations: \mathbf{M} is defined on configuration at time $t = -\infty$ while \mathbf{F}_{dp} maps configuration at time $t = t_{dp}$ to configuration at time t .

3. Results

Here we present results of simulations for the analytical model described in the previous section.

In the absence of energy limiter, i.e. intact material with $f_i = W_i$, the shape of the evolving aneurysms are shown in Figs. 2 and 3.

Simulations shown in Fig. 2 reproduce results of Kroon and Holzapfel (2007). It is important to note that in both cases aneurysms evolved gradually until they reached a steady shape. Material remained intact during the process.

Now, we enforce a failure description by introducing energy limiters in accordance with (5). In this case the bounded strain energy implies existence of a limit point on the stress-strain curve for fiber. The limit point designates the onset of fiber rupture. The latter, in its turn, triggers the overall aneurysm failure. A global indicator of the onset of aneurysm failure is singularity of the Hessian (the tangent stiffness matrix) of the total potential defined by (16). We remind the reader that though pressure load is generally non-conservative we have a conservative problem for the specific case of axisymmetric membrane. Singularity of the tangent stiffness matrix means the onset of failure that generally tends to localize into a crack. However, tracking the crack initiation and propagation are beyond the scope of the present work and we consider only the onset of failure.

Assuming that all collagen fibers are similar across the layers we calibrate the energy limiter value $\phi_i = \phi$ that corresponds to three different critical rupture stretches defined in uniaxial tension $\lambda_{cr} = 1.05, 1.10, 1.20$ for $\mu = 1 \times 10^7, 2 \times 10^7, 3 \times 10^7$ [N/m²]—Figs. 4–6. The range of the critical stretch from 1.05 to 1.20 probably covers all possible cases of fiber rupture. To the best of our knowledge no fibers reach 20% stretch without rupture. Of course, the considered range can be easily extended if necessary.

Then, we simulate the saccular (circular) and fusiform (cylindrical) aneurysm growth with the described fiber behavior for varying $\beta t_{lf} = 0.3, 0.45, 0.6$ and fixed $\alpha = 2$ and $\lambda_{pre} = 1.02$. The

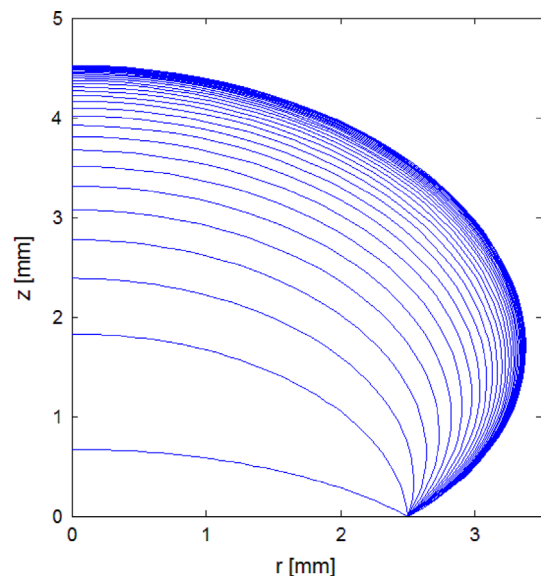


Fig. 2. Evolving plane membrane (saccular aneurysm).

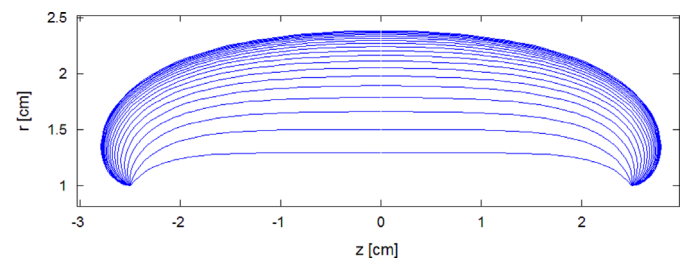


Fig. 3. Evolving cylindrical membrane (fusiform aneurysm).

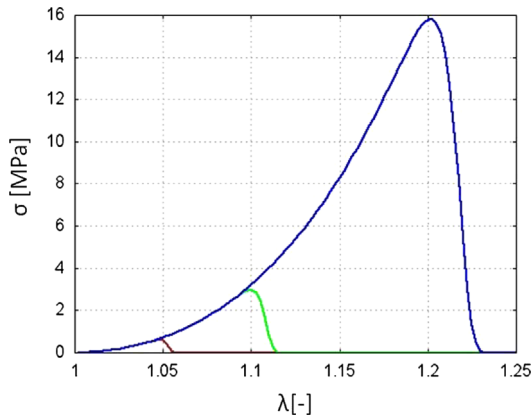


Fig. 4. Stress–stretch curve for individual fiber ($\mu = 1 \times 10^7$ [Pa]).

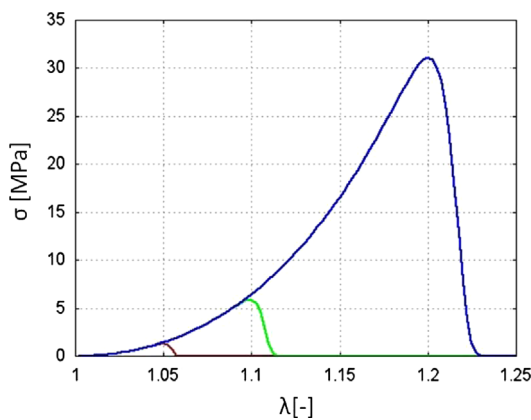


Fig. 5. Stress–stretch curve for individual fiber ($\mu = 2 \times 10^7$ [Pa]).

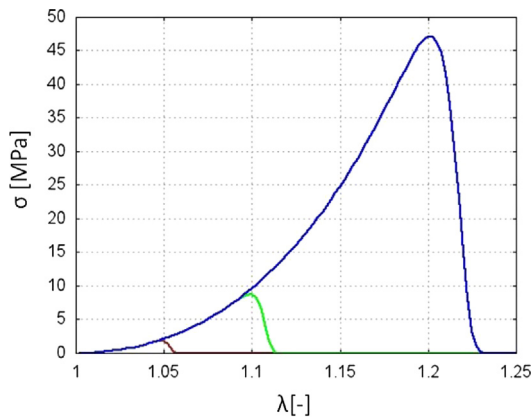


Fig. 6. Stress–stretch curve for individual fiber ($\mu = 3 \times 10^7$ [Pa]).

Table 2

Individual fiber parameters ($\mu = 2 \times 10^7$ [N/m²]) and saccular aneurysm rupture.

λ_{cr}	Φ [Pa]	σ_{max} [Pa]	$\beta t_{if} = 0.3$	$\beta t_{if} = 0.45$	$\beta t_{if} = 0.6$
1.05	2.90E+04	1.32E+06	rupture	rupture	rupture
1.10	2.35E+05	5.85E+06	rupture	rupture	rupture
1.20	3.10E+06	2.16E+07	rupture	intact	intact

Table 3

Individual fiber parameters ($\mu = 3 \times 10^7$ [N/m²]) and saccular aneurysm rupture.

λ_{cr}	Φ [Pa]	σ_{max} [Pa]	$\beta t_{if} = 0.3$	$\beta t_{if} = 0.45$	$\beta t_{if} = 0.6$
1.05	4.00E+04	2.10E+06	rupture	rupture	rupture
1.10	3.50E+05	8.70E+06	rupture	intact	intact
1.20	3.37E+06	4.72E+07	intact	intact	intact

Table 4

Individual fiber parameters ($\mu = 1 \times 10^7$ [N/m²]) and fusiform aneurysm rupture.

λ_{cr}	Φ [Pa]	σ_{max} [Pa]	$\beta t_{if} = 0.3$	$\beta t_{if} = 0.45$	$\beta t_{if} = 0.6$
1.05	1.30E+04	6.05E+05	rupture	rupture	rupture
1.10	1.20E+05	2.97E+06	rupture	intact	intact
1.20	1.13E+06	1.58E+07	intact	intact	intact

Table 5

Individual fiber parameters ($\mu = 2 \times 10^7$ [N/m²]) and fusiform aneurysm rupture.

λ_{cr}	Φ [Pa]	σ_{max} [Pa]	$\beta t_{if} = 0.3$	$\beta t_{if} = 0.45$	$\beta t_{if} = 0.6$
1.05	2.90E+04	1.32E+06	rupture	rupture	intact
1.10	2.35E+05	5.85E+06	intact	intact	intact
1.20	2.21E+06	2.16E+07	intact	intact	intact

Table 6

Individual fiber parameters ($\mu = 3 \times 10^7$ [N/m²]) and fusiform aneurysm rupture.

λ_{cr}	Φ [Pa]	σ_{max} [Pa]	$\beta t_{if} = 0.3$	$\beta t_{if} = 0.45$	$\beta t_{if} = 0.6$
1.05	4.00E+04	2.10E+06	rupture	intact	intact
1.10	3.50E+05	8.70E+06	intact	intact	intact
1.20	3.37E+06	4.72E+07	intact	intact	intact

Results of the simulation are shown in Tables 1–6. Two outcomes are observed: the aneurysm ruptures or remains intact. Inspecting the tables the reader can readily conclude that both outcomes can happen in accordance with the clinical observations.

4. Discussion

Most theoretical models describe evolution of aneurysms as a process dominated by degradation and deposition of collagen fibers. These models are short of a failure description that should be intrinsic part of the theory. This gap is amended in the present work in which failure of individual fibers is enforced by the method of energy limiters. The latter means that the strain energy accumulated by an individual fiber cannot exceed a certain

Table 1

Individual fiber parameters ($\mu = 1 \times 10^7$ [N/m²]) and saccular aneurysm rupture.

λ_{cr}	Φ [Pa]	σ_{max} [Pa]	$\beta t_{if} = 0.3$	$\beta t_{if} = 0.45$	$\beta t_{if} = 0.6$
1.05	1.30E+04	6.05E+05	rupture	rupture	rupture
1.10	1.20E+05	2.97E+06	rupture	rupture	rupture
1.20	1.13E+06	1.58E+07	rupture	rupture	rupture

choice of βt_{if} extends the one made by Kroon and Holzapfel (2007) and it can be explained by some scattering of the data on the collagen life time in the literature.

limit. Such limit characterizes the failure or bond energy. The existence of the energy bound implies a critical limit point on the stress-strain curve designating the onset of failure or rupture – Figs. 4–6. Thus, enforcing the energy limiter in the strain energy function we introduce a material failure description. The energy limiter approach can be applied to any model of growing intact aneurysm described in the literature. We chose the model proposed by Kroon and Holzapfel (2007) as the simplest one and modified it to include failure.

We applied the enhanced Kroon-Holzapfel model to simulations of evolving saccular and fusiform aneurysms. The former were modeled as circular axisymmetric membranes while the latter as the cylindrical axisymmetric ones. In the absence of reliable patient-specific data we performed parametric studies by varying the fiber stiffness, critical rupture stretch, deposition rate and lifetime. We tracked the singularity of the Hessian (the global tangent stiffness matrix) of the total potential. The singularity indicated the onset of the rupture process (crack formation and propagation), which was not tracked, however.

We found a range of parameters within which aneurysms stay intact or rupture. In choosing the range for parametric studies we stemmed from the data used by Kroon and Holzapfel (2007). We refer the reader to the latter paper for a detailed discussion which we do not duplicate here. It should not be missed also that our examples illustrate how the model works qualitatively. We neither make nor pretend making any specific quantitative predictions. Our purpose is to examine the possibility of modeling failure of growing aneurysms by using the proposed approach.

It is interesting to note that according to the obtained numerical results rupture occurs very quickly if it occurs at all. This qualitative result has experimental support. For example, Mitchell and Jakubowski (2000) conclude based on statistical analyses that cerebral aneurysms tend to rupture after a short period of intensive growth and those that survive are much less prone to rupture for a long period. Mathematically, fast rupture is a result of the assumption of constant energy limiter. Physically, it means that collagen fibers have the same constant strength during their life time and overall aneurysm rupture occurs due to the massive rupture of individual collagen fibers.

However, another scenario is possible and, probably, takes place for abdominal aortic aneurysm (Humphrey, 2002; Sakalihasan et al., 2005). In this case inter-fiber joints fail rather than individual fibers. Mathematically, it means that the energy limiter should be interpreted as an indicator of the inter-fiber joint strength, which should evolve during the aneurysm development (cf. Volokh and Vorp, 2008). Physically, it means that the overall aneurysm rupture is caused by disintegration of the fiber net rather than failure of individual fibers.

The present work explored a very simple model of aneurysm growth, remodeling, and failure. Obviously, this model can be further refined by including more constituents and considering realistic (patient-specific) geometries. Needless to say the present model can be incorporated in truly sophisticated theories accounting for the fluid-structure interaction. It was important here to show how a failure description can be a part of the constitutive theory and, thus, integrated in ‘first principles’ calculations. At the same time there is no doubt that experimental assessment of the micro-structure of the ruptured aneurysm could essentially guide further development of the macroscopic mathematical framework.

Conflict of interest

None declared.

Appendix A. Discretization

In this Appendix we discretize the problem in space and time. We partition the membrane into finite elements of equal length l_e and approximate functions within the e th element according to

$$R_e(\xi, t) = \frac{1}{2}\xi(\xi-1)R_{e1}(t) + (1-\xi^2)R_{e2}(t) + \frac{1}{2}\xi(\xi+1)R_{e3}(t) \quad (A.1)$$

$$r_e(\xi, t) = \frac{1}{2}\xi(\xi-1)r_{e1}(t) + (1-\xi^2)r_{e2}(t) + \frac{1}{2}\xi(\xi+1)r_{e3}(t) \quad (A.2)$$

$$z_e(\xi, t) = \frac{1}{2}\xi(\xi-1)z_{e1}(t) + (1-\xi^2)z_{e2}(t) + \frac{1}{2}\xi(\xi+1)z_{e3}(t) \quad (A.3)$$

$$\partial_\xi r_e(\xi, t) = \left(\xi - \frac{1}{2}\right)r_{e1}(t) - 2\xi r_{e2}(t) + \left(\xi + \frac{1}{2}\right)r_{e3}(t) \quad (A.4)$$

$$\partial_\xi z_e(\xi, t) = \left(\xi - \frac{1}{2}\right)z_{e1}(t) - 2\xi z_{e2}(t) + \left(\xi + \frac{1}{2}\right)z_{e3}(t) \quad (A.5)$$

where $\xi \in [-1, 1]$ is a local coordinate; and $R_{ei}(t)$, $r_{ei}(t)$, $z_{ei}(t)$ are the time-dependant nodal values of $R_e(\xi, t)$, $r_e(\xi, t)$, $z_e(\xi, t)$ accordingly.

Noticing that

$$dS = l_e d\xi, \quad (\dots)' = \frac{1}{l_e} \partial_\xi (\dots) \quad (A.6)$$

we calculate

$$r'_e(\xi, t) = \frac{1}{l_e} \left\{ \left(\xi - \frac{1}{2}\right)r_{e1}(t) - 2\xi r_{e2}(t) + \left(\xi + \frac{1}{2}\right)r_{e3}(t) \right\} \quad (A.7)$$

$$z'_e(\xi, t) = \frac{1}{l_e} \left\{ \left(\xi - \frac{1}{2}\right)z_{e1}(t) - 2\xi z_{e2}(t) + \left(\xi + \frac{1}{2}\right)z_{e3}(t) \right\} \quad (A.8)$$

The squared stretches of the membrane element (18)_{1,2} take form

$$\lambda_{1e}^2(\xi, t) = r_e^2(\xi, t) + z_e^2(\xi, t), \quad \lambda_{2e}^2(\xi, t) = r_e^2(\xi, t)/R_e^2(\xi, t) \quad (A.9)$$

Then, the total energy of the element can be written as follows

$$\Pi = \int_{-1}^1 \Pi_e d\xi \quad (A.10)$$

$$\Pi_e = \pi \int_{-1}^1 (2R_e \sum_{i=1}^n h_{ie} \psi_{ie} + p r_e^2) l_e d\xi \quad (A.11)$$

Integrating the previous expression at two Gauss points: $\xi_1 = -1/\sqrt{3}$ and $\xi_2 = 1/\sqrt{3}$ we get the spatial approximation

$$\begin{aligned} \Pi_e(t) \approx & \pi l_e \{ 2R_e(\xi_1, t) \sum_{i=1}^n h_{ie} \psi_{ie}(\xi_1, t) + p r_e^2(\xi_1, t) z'_e(\xi_1, t) \} \\ & + \pi l_e \{ 2R_e(\xi_2, t) \sum_{i=1}^n h_{ie} \psi_{ie}(\xi_2, t) + p r_e^2(\xi_2, t) z'_e(\xi_2, t) \} \end{aligned} \quad (A.12)$$

It remains only to discretize the element potential in time. For this purpose we consider the discrete time increments $\Delta t_j = t_j - t_{j-1}$ and approximate the strain energy of the element of the i^{th} layer by the sum

$$\psi_{ie}(\xi_\nu, t_k) = \sum_{j=k-n^*}^k \dot{m}_{ie}(\xi_\nu, t_j) f_{ie}(\xi_\nu, t_k, t_j) \Delta t_j \quad (A.13)$$

where $\nu = 1, 2$ and n^* is the number of the time discretization points of the life cycle t_{lf} .

We assume that the loading and remodeling start at $k = 0$.

Thus, we have for $j > 0$:

$$\dot{m}_{ie}(\xi_\nu, t_j) = \beta \{ \lambda_{1e}^2(\xi_\nu, t_j) \cos^2 \phi_i + \lambda_{2e}^2(\xi_\nu, t_j) \sin^2 \phi_i \}^\alpha \quad (A.14)$$

$$W_{ie}(\xi_\nu, t_k, t_j) = \mu \left\{ \lambda_{pre}^2 \frac{\lambda_{1e}^2(\xi_\nu, t_k) \cos^2 \phi_i + \lambda_{2e}^2(\xi_\nu, t_k) \sin^2 \phi_i - 1}{\lambda_{1e}^2(\xi_\nu, t_j) \cos^2 \phi_i + \lambda_{2e}^2(\xi_\nu, t_j) \sin^2 \phi_i} \right\}^3 \quad (A.15)$$

There is no stretching for $j \leq 0$:

$$\dot{m}_{ie}(\xi_\nu, t_j) = \beta \quad (\text{A.16})$$

$$W_{ie}(\xi_\nu, t_k, t_j) = \mu \{ \lambda_{pre}^2 (\lambda_{1e}^2(\xi_\nu, t_k) \cos^2 \phi_i + \lambda_{2e}^2(\xi_\nu, t_k) \sin^2 \phi_i) - 1 \}^3 \quad (\text{A.17})$$

References

- Baek, S., Rajagopal, K.R., Humphrey, J.D., 2006. A theoretical model of enlarging intracranial fusiform aneurysms. *J. Biomech. Engng.* 128, 142–149.
- Bengtsson, H., Sonesson, B., Bergqvist, D., 1996. Incidence and prevalence of abdominal aortic aneurysms, estimated by necropsy studies and population screening by ultrasound. *Ann. NY. Acad. Sci.* 800, 1–24.
- Chatziprodromou, I., Tricoli, A., Poulikakos, D., Ventikos, Y., 2007. Hemodynamic and wall remodeling of a growing cerebral aneurysm: A computational model. *J. Biomech.* 40, 412–426.
- Figueroa, C.A., Baek, S., Taylor, C.A., Humphrey, J.D., 2009. A computational framework for fluid-solid-growth modeling in cardiovascular simulations. *Comput. Methods Appl. Mech. Eng.* 198, 3583–3602.
- Fried, I., 1982. Finite element computation of large rubber membrane deformations. *Int. J. Numer. Methods Eng.* 18, 653–660.
- Humphrey, J.D., 2002. *Cardiovascular Solid Mechanics: Cells, Tissues, and Organs*. Springer, New York.
- Humphrey, J.D., Rajagopal, K.R., 2002. A constrained mixture model for growth and remodeling of soft tissues. *Math. Models Methods Appl. Sci.* 12, 407–430.
- Humphrey, J.D., Taylor, C.A., 2008. Intracranial and abdominal aortic aneurysms: similarities, differences, and need for a new class of computational models. *Annu. Rev. Biomed. Eng.* 10, 221–246.
- Kroon, M., Holzapfel, G.A., 2007. A model of saccular cerebral aneurysm growth by collagen fiber remodeling. *J. Theor. Biol.* 247, 775–787.
- Kroon, M., Holzapfel, G.A., 2008. Modeling of saccular aneurysm growth in a human middle cerebral artery. *J. Biomech. Eng.* 130, 051012.
- Kroon, M., Holzapfel, G.A., 2009. A theoretical model for fibroblast-controlled growth of saccular cerebral aneurysm. *J. Theor. Biol.* 257, 73–83.
- Martufi, G., Gasser, T.C., 2012. Turnover of fibrillar collagen in soft biological tissue with application to the expansion of abdominal aortic aneurysms. *J. R. Soc. Interface* 9, 3366–3377.
- Mitchell, P., Jakubowski, J., 2000. Estimate of the maximum time interval between formation of cerebral aneurysm and rupture. *J. Neurol. Neurosurg. Psychiatry* 69, 760. (-167).
- Ouriel, K., Green, R.M., Donayre, C., Shortell, C.K., Elliott, J., DeWeese, J.A., 1992. An evaluation of new methods of expressing aortic aneurysm size: relationship to rupture. *J. Vasc. Surg.* 15, 12–20.
- Patel, M.I., Hardman, D.T., Fisher, C.M., Appleberg, M., 1995. Current views on the pathogenesis of abdominal aortic aneurysms. *J. Am. Coll. Surg.* 181, 371–382.
- Sakalihasan, N., Limet, R., Defawe, O.D., 2005. Abdominal aortic aneurysm. *Lancet* 365, 1577–1589.
- Schmid, H., Watton, P.N., Maurer, M.M., Wimmer, J., Winkler, P., Wang, Y.K., Rohrlé, O., Itskov, M., 2010. Impact of transmural heterogeneities on arterial adaptation: Application to aneurysm formation. *Biomech. Model. Mechanobiol.* 9, 295–315.
- Volokh, K.Y., Vorp, D.A., 2008. A model of growth and rupture of abdominal aortic aneurysm. *J. Biomech.* 41, 1015–1021.
- Volokh, K.Y., 2011. Modeling failure of soft anisotropic materials with application to arteries. *J. Mech. Behav. Biomed. Mater.* 4, 1582–1594.
- Volokh, K.Y., 2013. Review of the energy limiters approach to modeling failure of rubber. *Rubber Chem. Technol.* 86, 470–487.
- Watton, P.N., Hill, N.A., 2009. Evolving mechanical properties of a model of abdominal aortic aneurysm. *Biomech. Model. Mechanobiol.* 8, 25–42.
- Watton, P.N., Hill, N.A., Heil, M., 2004. A mathematical model for the growth of the abdominal aortic aneurysm. *Biomech. Model. Mechanobiol.* 3, 98–113.
- Watton, P.N., Selimovic, A., Raberger, N.B., Huang, P., Holzapfel, G.A., Ventikos, Y., 2011. Modeling evolution and the evolving mechanical environment of saccular cerebral aneurysms. *Biomech. Model. Mechanobiol.* 10, 109–132.
- Watton, P.N., Ventikos, Y., Holzapfel, G.A., 2009. Modeling the growth and stabilization of cerebral aneurysm. *Math. Medicine Biol.* 26, 133–164.